

# Pre-Determination and Experimental Verification of Voltage Regulation from the Output Equivalent Circuit in a Forced Resonant Inductive Coupled Wireless Power Transfer System

\*Hema Ramachandran, \*\*Bindu G.R

\*Department of Electrical Engineering, College of Engineering, University of Kerala  
Thiruvananthapuram, Kerala, India (hemaachuth@gmail.com)

\*\*Department of Electrical Engineering, University of Kerala,  
Thiruvananthapuram, Kerala, India (bgr100@gmail.com)

## Abstract

An analytical two port lumped element network model of a resonant inductive coupled wireless power transfer system with helical solenoid geometry is developed to formulate its input and output equivalent circuits. The lumped element network is developed as a consolidation of various distributed elements spatially distributed throughout the length of the helical solenoid geometry. The generated lumped element network uses the near field criterion that the physical length of the wires forming the entire network is less than the wavelength of operation of the circuit. The two port network is analysed using Z parameters without source and load to determine the driving and transfer impedances. With source and load connected, the input and output equivalent circuits are developed. The output equivalent circuit is used to predetermine the voltage regulation of the near field system. Experimental verification of voltage regulation of the wireless power transfer system is performed at a forced resonant frequency of 1.2MHz. The analytical model is in close agreement with the experimental results.

**Key words:** Wireless power transfer system model, near-field coupling, high frequency power system, air-core transformer model, voltage regulation

## 1. Introduction

Many of the recent research into resonant inductive coupling in wireless power transfer systems focus on improving the performance using varying coil geometries (Alanson P. Sample *et al*, 1991). Development of a dynamic system model is essential for analyzing the performance of the system at resonant frequency of the transmitter and receiver coils in these systems.

Moreover, an in-depth study of coil geometry is required as the parameters of the system are significantly influenced by coil geometry (Mizuno T *et al*, 2011). Solenoid geometries are the most commonly used coils operating in a wide range from a few KHz to 20MHz (J.G. Zhu *et al*, 1996). The coils used are cylindrical air-cored and have diameter of the coils larger than the length. Various network topologies are also in use for realizing these systems (C.S. Wang *et al*, 2004). Since these systems operate in the near field region of wavelength  $\lambda$  ranging from 15-3000m, the use of an appropriate element model is also necessary. After careful consideration of the past investigations, it has been found that an analytical model for the resonant inductive coupled power transfer system based on helical solenoid geometry which accounts for the distributed effects has not been formulated. From the developed analytical model the voltage regulation of the system is pre-determined from its output equivalent circuit.

This paper is organized as follows: The development of a high frequency reflected impedance terminal model using Parallel-Parallel (PP) network topology with top coupling incorporating distributed effects of all the parameters of the transmitter and receiver coils consolidated to a lumped element model is presented in Section 2. Formulation of a two port network from the developed analytical model is presented in section 3. The development of input and output equivalent circuits for the pre-determination of voltage regulation is presented in Section 4. Section 5 discusses the experimental verification of voltage regulation at 1.2MHz forced resonant frequency.

## **2. Development of High Frequency Reflected Impedance Terminal Transformer Model employing Parallel-Parallel Topology with Top Coupling**

The transmitter and receiver coils in the wireless power transfer system are air cored coils with helical geometry and power transmission is enabled through air. The coupling between the coils is very small and most of the inductance is leakage. The flux and current relationship is linear, due to large magnetizing current required for transmission. Resonant inductive coupled linear high frequency transformer model is established by creating forced resonant LC circuits in the primary and secondary loosely coupled circuits and transferring power using electromagnetic coupling. A magneto quasi static interaction between the transmitter and receiver coils have been assumed with receiver coil displaced at a distance  $d$  from the near field of the transmitter coil obeying the inequality  $d < \lambda/2\pi$ .

The authors have developed the lumped element model of the helical single layer solenoid by merging the distributed element models between the turns as in Fig.1 (a) of a single layer solenoid. The distributed element model considers the inductance between the turns  $L_{turn}$  by

subtracting inductance for insulation space. Along with this, the internal inductance contribution due to skin effect  $L_i$  and lead wire inductance  $L_l$  effect has been taken into account. The distributed element model has been consolidated for the solenoid and has been rolled up into a single lumped element inductance  $L$ . Similarly the overall effects of distributed capacitance between the turns and turn to ground capacitance forming  $C_{turn}$ , along with lead wire capacitance  $C_l$  has been considered as a single lumped capacitance  $C$  in parallel with the coil. The distributed effects of resistance between the turns in series  $R_{DC}$  with distributed resistance due to skin and proximity effect  $R_{AC}$  and radiative resistance  $R_{rad}$  has been combined into a single resistance  $R$  for the whole coil. This lumped model as in Fig.1(b) is appropriate since the circuit length is less than the wavelength.

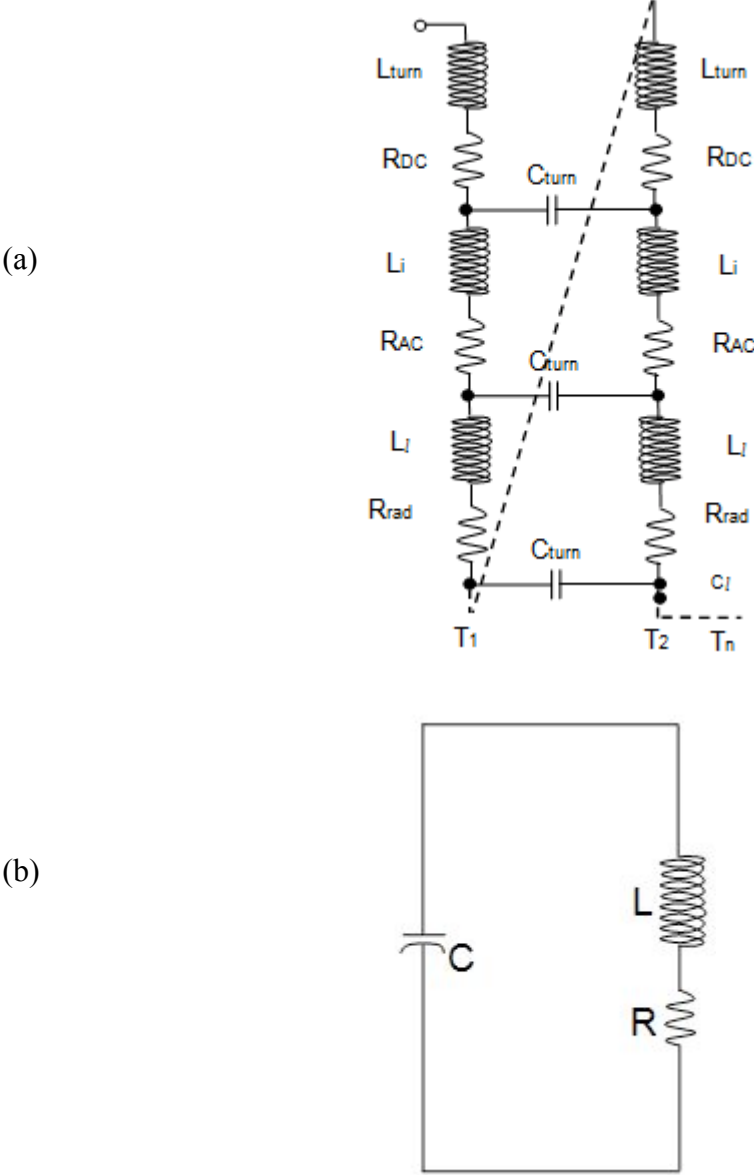


Fig.1(a) The distributed model incorporating distributed effects of inductance, resistance and capacitance.

(b). Consolidated lumped element model generated from the distributed element model, where

$$\text{the elements are } L = \sum_{l=1}^n L_{lum} + L_i + L_l, C = \sum_{l=1}^n C_{lum} + C_l, R = \sum_{l=1}^n R_{DC} + R_{AC} + R_{rad}$$

The self-inductances  $L_T$  and  $L_R$  with its parasitic coil resistances  $R_T$  and  $R_R$  and the distributed parasitic capacitances  $C_T$  and  $C_R$  of the transmitter and receiver coils are consolidated based on the formulation in Fig.1 (b), to form a lumped terminal network. With physical arrangement of the capacitances deciding the topology of the network, a Parallel-Parallel topology (PP) (O.H. Stielau *et al*, 2000) has been identified for the linear high frequency transformer model. When the transmitter coil is energized from a high frequency alternating voltage source  $V_s$  having internal resistance  $R_s$ , mutual inductance  $M_{TR}(d)$  is established between the transmitter and receiver coils, which is a function of coil position, size and geometry. Accumulation of electrostatic charges around the coils produces a mutual capacitance  $C_{TR}(d)$  or Top couplings which vary with distance between the coils. The developed model for resonant inductive wireless power transfer system can be identified as PP network topology with top coupling. It has all the functional capabilities of high frequency reflected impedance linear terminal transformer model and is presented in Fig. 2.

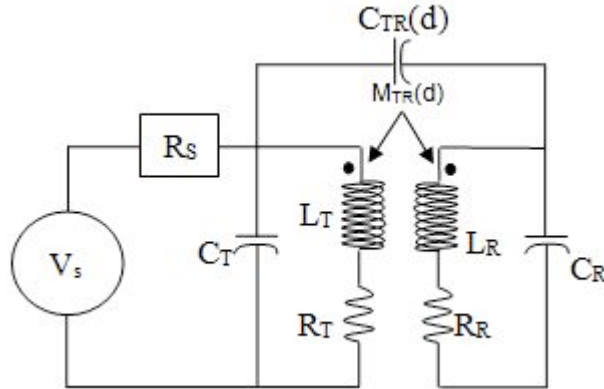


Fig.2. Analytical reflected impedance terminal transformer model of the wireless power transfer system using PP network topology with top coupling.

The self-inductances of the transmitter and receiver coils developed by the authors for the helical solenoid  $L_T$  and  $L_R$ , where the first factor is the Nagaoka self-inductance which takes into account the effect of the ends for long solenoids, second is deduction of correction for insulation space for helices of round wire, third and fourth factors are internal inductance contribution and lead wire contribution and is given by

$$L_{self} = \frac{k\mu_0 AN^2}{l} - \mu_0 r N \left( \left( \frac{5}{4} - \ln(\tan \varphi) \right) - \frac{3}{2} \ln \frac{N}{6N} - \frac{0.3308}{N} \right) + \mu_0 l_w \left( \frac{\delta}{2\pi d_w} + 0.2 \times 10^{-9} \left( \ln \frac{4l_w}{d_w} - 0.75 \right) \right) \quad (1)$$

The self-capacitances of the transmitter and receiver coils  $C_T$  and  $C_R$  are found where the first factor is the consolidated self-capacitance between the turns of a coil which also includes the capacitance between the turns and ground and the second factor is the capacitance due to lead wires and is given by

$$C_{self} = \frac{4r^2 N^2 \varepsilon_0 \mu_0 \left( 1 + 0.7096 \left( \frac{D}{l} \right) + 2.3950 \left( \frac{D}{l} \right)^{1.5} \right)}{L_{self} \cos^2 \varphi} + \left( \frac{0.55 \varepsilon_0 l_w}{\ln \left( \frac{h}{d_w} \right)} \right) \times 10^{-10} \quad (2)$$

The mutual inductance  $M_{TR}(d)$  (J.E. Clem, 1927) between the receiver coil of radius  $a$ , length  $2m_1$ , turns per unit length  $n_1$  and the transmitter coil of radius  $A$ , length  $2m_2$  and turns per unit length  $n_2$  separated by a small distance  $d$  is found from the transformer model, where

$r_n = \sqrt{A^2 + x_n^2}$  and  $B_n$  are functions which depend on  $\frac{A^2}{r_n^2}$  and  $\frac{a}{A}$ , and is given by

$$M_{TR}(d) = 0.002\pi^2 a^2 n_1 n_2 [r_1 B_1 - r_2 B_2 - r_3 B_3 + r_4 B_4] \quad (3)$$

The capacitance  $C_{TR}(d)$  in between the parallel round conductors situated in air, neglecting their insulation coating (Marian K. Kazimierczuk, 2009), where  $d_c$  is the distance between the centres of the two conductors is given by

$$C_{TR}(d) = \frac{\pi^2 \varepsilon_0 D}{\cosh^{-1} \left( \frac{d_c}{d_w} \right)} \quad (4)$$

The AC resistance due to skin and proximity effect and the second is the radiation resistance of an ideal Hertzian dipole and is given by

$$R_p = \phi_{AC} \phi_M R_{DC} + R_{rad} = \left( 0.4984 \left( \frac{r_w}{\delta} \right) + 0.264 \right) \times \left( \frac{p/d_w}{(l_w/D)} \right) \times \frac{\rho l_w}{\pi r_w^2} + \frac{2\pi}{3} \eta_0 \left( \frac{l}{\lambda} \right)^2 \quad (5)$$

### 3. Development of Two Port Network

The reflected impedance terminal model is further reduced using circuit transformation and reduction techniques to a  $\pi$  equivalent network. The  $\pi$  equivalent network (Kang Lin *et al*, 2009) is represented in the form of a two port network. The circuit transformation and reduction techniques are summarized below.

### 3.1 Voltage Source $V_s$ to Current Source $I_1$ Transformation

The first reduction of the reflected impedance model involves converting the constant voltage source  $V_s$  to constant current source  $I_1$  using voltage source to current source transformation. The current source  $I_1$  is shown in Fig.3 (a), the value of which is given by

$$I_1 = \frac{V_s}{R_s} \quad (6)$$

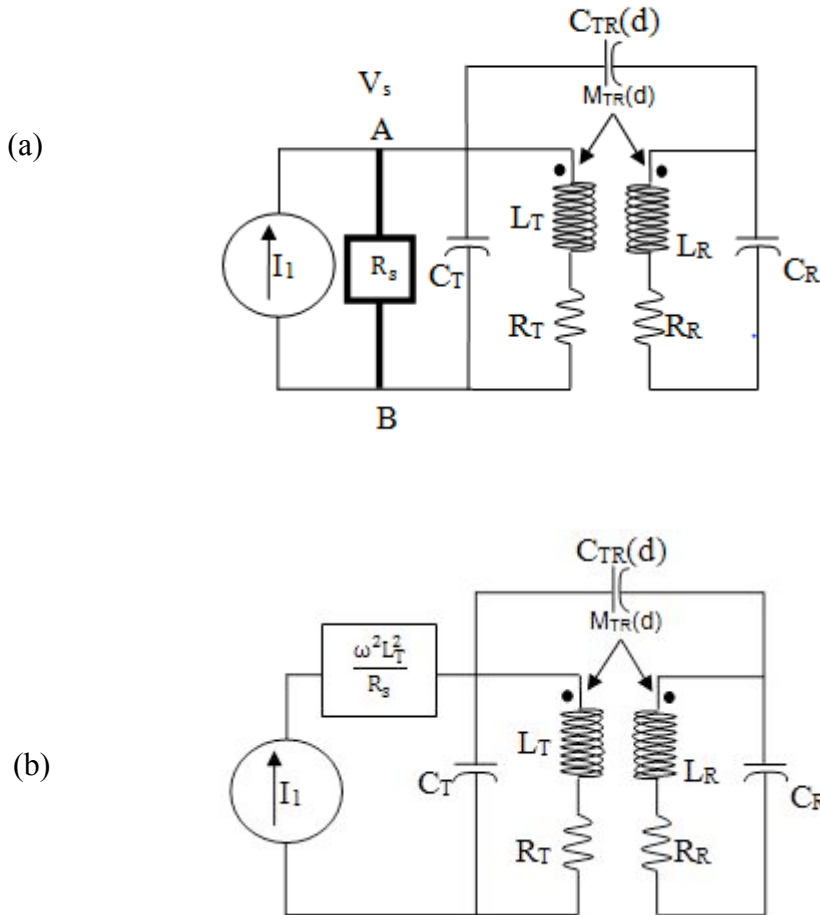


Fig.3 (a) Current source  $I_1$  in parallel with internal resistance  $R_s$ .

(b) Parallel resistance  $R_s$  converted to series resistance  $\frac{\omega^2 L_T^2}{R_s}$

### 3.2 Conversion of Parallel Resistance $R_s$ to Series Resistance

From circuit theory, any series circuit consisting of inductance  $L_s$  and resistance  $R_s$  series circuit can be converted to its equivalent parallel circuit of inductance  $L_p$  and resistance  $R_p$  by equating their admittances and is given by

$$R_p = \frac{R_s^2 + \omega^2 L_s^2}{R_s} = R_s + \frac{\omega^2 L_s^2}{R_s} \quad (7)$$

The Quality factor also called the unloaded Q of the coil, which is a measure of purity of the inductance is defined as the ratio of coil reactance to resistance and is given by.

$$Q = \frac{\omega L_s}{R_s} \quad (8)$$

Since the coil quality factor Q is very large ( $\omega L_s \gg R_s$ ) in the frequency range of operation, the modified form is given by

$$R_p = \frac{\omega^2 L_s^2}{R_s} \quad (9)$$

The parallel resistance  $R_s$  of the resonant wireless power transfer model in Fig.3 (a) is converted to series resistance  $R_{series}$  and the conversion is shown in Fig.3 (b).

$$R_{series} = \frac{\omega^2 L_T^2}{R_s} \quad (10)$$

### 3.3 Current Source $I_1$ to Voltage Source Transformation

The Norton current source  $I_1$  is then converted to Thevenin voltage source  $\frac{-jV_s}{R_s \omega C_T}$ , by multiplying with the parallel impedance  $\frac{1}{j\omega C_T}$ . The conversion is represented in Fig.4 (a). This voltage source is in series with  $C_T$  given by

$$I_1 \times \frac{1}{j\omega C_T} = \frac{V_s}{R_s} \times \frac{1}{j\omega C_T} = \frac{-jV_s}{R_s \omega C_T} \quad (11)$$

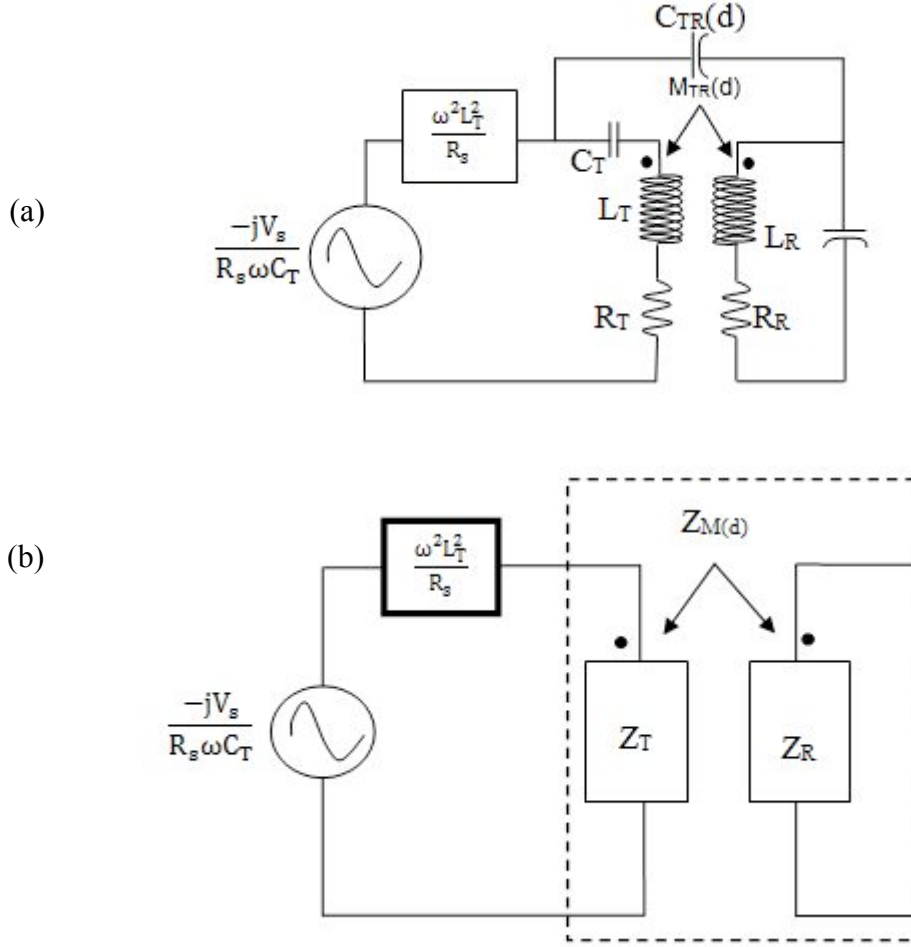


Fig4 (a). Current source  $I_1$  converted to voltage source which is in series with  $C_T$  .  
 (b) Representation of coupling part in dotted box of the resonant wireless power transfer system in terms of impedances.

### 3.4 Equivalent Impedances of the Magnetically Coupled part of the Wireless Power Transfer System

The magnetic coupling part of the resonant coupled wireless power transfer system shown in dotted box with impedances as shown in Fig.4 (b). The impedance of the transmitter coil  $Z_T$ , the impedance on the receiver coil  $Z_R$  with the mutual impedance  $Z_M(d)$ , varying with distance can be represented as follows.

$$Z_T = R_T + j\omega L_T + \frac{1}{j\omega C_T} \quad (12)$$

$$Z_R = \frac{R_R + j\omega L_R}{1 + j\omega C_R (R_R + j\omega L_R)} \quad (13)$$

$$Z_M(d) = \frac{j\omega M_{TR}(d) \times \frac{1}{j\omega C_{TR}(d)}}{j\omega M_{TR}(d) + \frac{1}{j\omega C_{TR}(d)}} = \frac{j\omega M_{TR}(d)}{1 - \omega^2 M_{TR}(d)C_{TR}(d)} \quad (14)$$

### 3.5. Magnetically Coupled part of the Wireless Power Transfer System converted to a $\pi$ Equivalent Network.

The resonant inductive coupled wireless power transfer model of Fig.4 (b) is then converted to a  $\pi$  equivalent network to remove the magnetic coupling between the transmitter and receiver coils. With a common ground imposed on the coupled circuits, the voltage current relationships give the matrix equation given by

$$\begin{bmatrix} V_1 \\ V_2 \end{bmatrix} = \begin{bmatrix} Z_T & Z_M(d) \\ Z_M(d) & Z_R \end{bmatrix} \begin{bmatrix} I_1 \\ I_2 \end{bmatrix} \quad (15)$$

Equation (15) on matrix inversion is given by

$$\begin{bmatrix} I_1 \\ I_2 \end{bmatrix} = \begin{bmatrix} \frac{Z_R}{j\omega(Z_T Z_R - (Z_M(d))^2)} & \frac{-Z_M(d)}{j\omega(Z_T Z_R - (Z_M(d))^2)} \\ \frac{-Z_M(d)}{j\omega(Z_T Z_R - (Z_M(d))^2)} & \frac{Z_T}{j\omega(Z_T Z_R - (Z_M(d))^2)} \end{bmatrix} \begin{bmatrix} V_1 \\ V_2 \end{bmatrix} \quad (16)$$

The  $\pi$  equivalent network replacing the coupled part of the wireless power transfer system model is represented in Fig.5 (a). The voltages across the nodes 1 and 2 are represented as  $V_1$  and  $V_2$  and the corresponding currents flowing into the nodes are  $I_1$  and  $I_2$ . Nodal analysis at 1 and 2 the terminal equations can be represented as

$$\begin{bmatrix} I_1 \\ I_2 \end{bmatrix} = \begin{bmatrix} \frac{1}{j\omega Z_A} + \frac{1}{j\omega Z_C} & \frac{-1}{j\omega Z_C} \\ \frac{-1}{j\omega Z_C} & \frac{1}{j\omega Z_B} + \frac{1}{j\omega Z_C} \end{bmatrix} \begin{bmatrix} V_1 \\ V_2 \end{bmatrix} \quad (17)$$

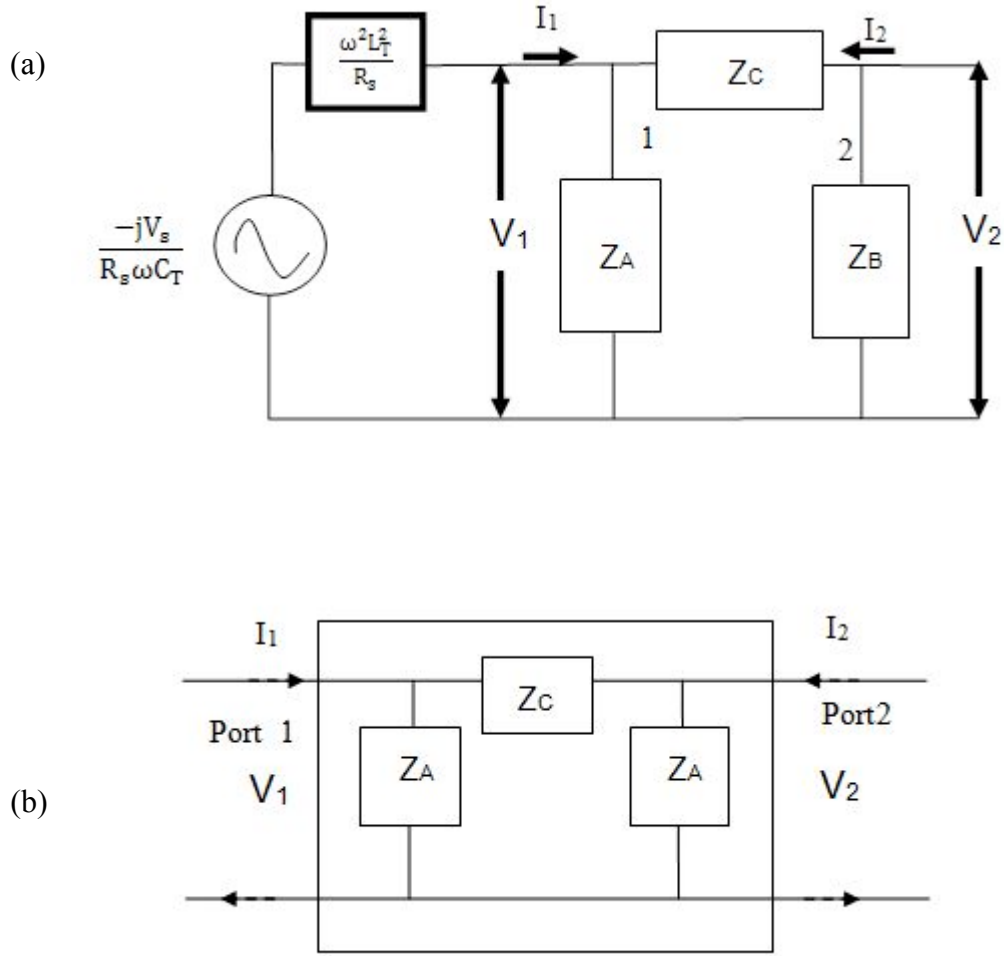


Fig.5 (a).The  $\pi$  equivalent network on the coupled part of the wireless power transfer system.

(b) Two port network model of the power transfer system without source and load

Equation (16) and (17) are representations of admittance matrices of the coupling part of Fig.4 (b) and Fig.5 (a). These admittance matrices are equated to get the impedance of the  $\pi$  equivalent network represented by  $Z_A$ ,  $Z_B$  and  $Z_C$ .

$$Z_A = \frac{Z_T Z_R - (Z_M(d))^2}{Z_R - Z_M(d)} \quad (18)$$

$$Z_B = \frac{Z_T Z_R - (Z_M(d))^2}{Z_T - Z_M(d)} \quad (19)$$

$$Z_C = \frac{Z_T Z_R - (Z_M(d))^2}{Z_M(d)} \quad (20)$$

### 3.6. The Two Port Network Model

The  $\pi$  equivalent network (Kang Lin, 2009) is finally represented by a two port network. The two-port network model of the wireless power transfer system was analysed without source and load and is shown in Fig. 5(b). The Z parameters of the two ports without source and load are found by open circuit tests on both the ports and are represented in Table I.

Table I. Z Parameters of the Two Port Resonant Coupled System

2 –port condition	Equivalent terminal impedance at ports
$\frac{V_1}{I_1}   I_2 = 0$	$Z_{11} = \frac{Z_A(Z_B + Z_C)}{Z_A + Z_B + Z_C}$
$\frac{V_1}{I_2}   I_1 = 0$	$Z_{12} = \frac{Z_A Z_B}{Z_A + Z_B + Z_C}$
$\frac{V_2}{I_1}   I_2 = 0$	$Z_{21} = \frac{Z_A Z_B}{Z_A + Z_B + Z_C}$
$\frac{V_2}{I_2}   I_1 = 0$	$Z_{22} = \frac{Z_B(Z_A + Z_C)}{Z_A + Z_B + Z_C}$

#### 4. Development of Input Equivalent Circuit and Pre-Determination of Voltage Regulation from Output Equivalent Circuit

##### 4.1. Two port connected to source and load

When the two port network is connected to source and load  $R_L$ , the two port network with input impedance  $Z_{in}$  and output impedance  $Z_{ou}$  are represented as in Fig.6. In the characterisation of the two port, the output port current ( $-I_2$ ) is measured as leaving port 2.

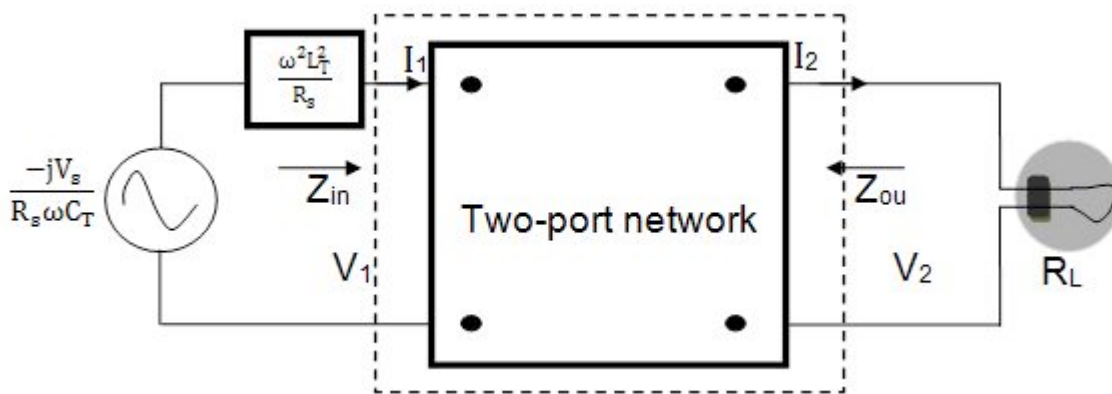


Fig.6. The two port network connected to source  $\frac{-jV_s}{R_s \omega C_T}$  and load  $R_L$

The impedance matrix equations as viewed from the input side (port1) of the two port with load connected to port 2 is represented as follows.

$$V_1 = Z_{11}I_1 - Z_{12}I_2 \quad (21)$$

$$V_2 = Z_{21}I_1 - Z_{22}I_2 = R_L I_2 \quad (22)$$

The value of  $I_2$  is given by

$$I_2 = \frac{Z_{21}I_1}{Z_{22} + R_L} \quad (23)$$

Substituting the value of  $I_2$  in equation (21), to get the representation of input impedance  $Z_{in}$  as follows:

$$V_1 = \left( Z_{11} - \frac{Z_{12}Z_{21}}{Z_{22} + R_L} \right) I_1 = Z_{in} I_1 \quad (24)$$

$$Z_{in} = \left( Z_{11} - \frac{Z_{12}Z_{21}}{Z_{22} + R_L} \right) \quad (25)$$

Equation (25) gives an account of the input impedance of the transmitter coil viewed from the input side of the two port. The impedance consists of the inherent impedance of the transmitter coil  $Z_{11}$  along with the reflected impedance from the receiver coil. The output impedance  $Z_{ou}$  is determined by reversing the roles of supply and load with voltage source shorted. The impedance matrix equations represented by

$$0 - \frac{\omega^2 L_T^2}{R_s} I_1 = Z_{11}I_1 - Z_{12}I_2 \quad (26)$$

$$V_2 = Z_{21}I_1 - Z_{22}I_2 \quad (27)$$

Equation (26) is re-arranged to get

$$I_2 = \frac{Z_{12}I_1}{Z_{11} + \frac{\omega^2 L_T^2}{R_s}} \quad (28)$$

Substituting the value of  $I_1$  in (27) to get (29).

$$V_2 = \frac{Z_{12}Z_{21}I_2}{Z_{11} + \frac{\omega^2 L_T^2}{R_s}} - Z_{22}I_2 = \left( \frac{Z_{12}Z_{21}}{Z_{11} + \frac{\omega^2 L_T^2}{R_s}} - Z_{22} \right) I_2 \quad (29)$$

The output impedance is given by

$$Z_{ou} = \frac{V_2}{-(I_2)} = Z_{22} - \frac{Z_{12}Z_{21}}{Z_{11} + \frac{\omega^2 L_T^2}{R_s}} \quad (30)$$

Equation (30) gives an account of the output impedance of the receiver coil viewed from the output side of the two port. The impedance consists of the inherent impedance of the receiver coil  $Z_{22}$  and the reflected impedance from the transmitter coil.

#### 4.2. Development of Input and Output Equivalent Circuits

The input and output impedances pre-determined in section 4.1 enables to replace the two port of Fig.6 by input and output equivalent circuits. The two port and the load is replaced by the input impedance  $Z_{in}$  connected at port 1. The value of  $Z_{in}$  is given by equation (25). The source voltage, the transformed source resistance along with the input impedance  $Z_{in}$  and the port1 current  $I_1$ , has been reduced to a single circuit to form the input equivalent circuit. The input equivalent circuit as seen from the transmitter coil end is shown in Fig.7.

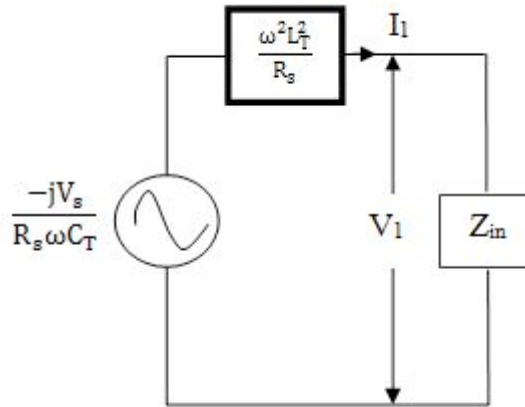


Fig.7. The input equivalent circuit of the resonant inductive wireless power transfer system.

The source and the two port can be replaced by Thevenin equivalent circuit connected at port 2. The Thevenin open circuit voltage is obtained with load open circuit ( $I_2=0$ ) from the mesh equations at port 1.

$$\frac{-jV_s}{R_s \omega C_T} - \frac{\omega^2 L_T^2}{R_s} I_1 = Z_{11} I_1 \quad (31)$$

$$V_{th} = V_2 = Z_{21} I_1 \quad (32)$$

$$V_{th} = Z_{21} I_1 = \frac{-jV_s}{Z_{11} + \frac{\omega^2 L_T^2}{R_s}} \times \frac{Z_{21}}{Z_{11} + \frac{\omega^2 L_T^2}{R_s}} \quad (33)$$

The Thevenin Impedance  $Z_{th}$  is the output impedance  $Z_{ou}$  obtained from equation (30), with input voltage shorted.

$$Z_{th} = Z_{ou} = Z_{22} - \frac{Z_{21}}{Z_{11} + \frac{\omega^2 L_T^2}{R_s}} \quad (34)$$

The load voltage  $V_2$  can be determined from the load resistance  $R_L$  and Thevenin impedance  $Z_{th}$ . The short circuit current at port 2 in terms of load voltage  $V_2$  and load impedance  $R_L$  is given as follows:

$$V_2 = \frac{V_{th}}{Z_{th} + R_L} \quad (35)$$

$$I_2 = \frac{V_2}{R_L} \quad (36)$$

The Thevenin equivalent circuit also called as the output equivalent circuit is represented in Fig.8.

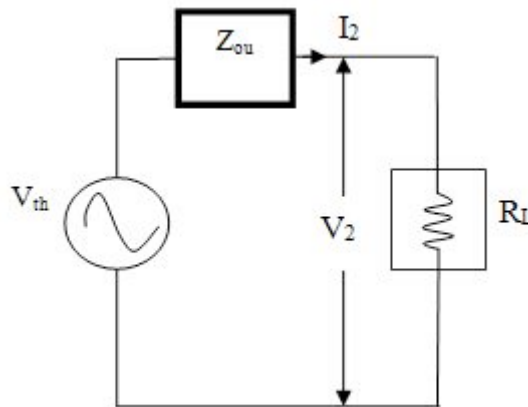


Fig.8. The output equivalent circuit of the wireless power transfer system.

#### 4.4. Pre-determination of Voltage Regulation from the Output Equivalent Circuit

Voltage regulation of the wireless power transfer system is pre-determined by the authors from the output equivalent circuit. It is the percentage change in the output voltage from no-loading of the receiver coil to full-loading of the receiver coil. The voltage regulation of the system is analogous to a transformer and is dynamic and load-dependent. The open circuit voltage across the receiver is  $V_{th}$  and is given by equation (33). With a resistive load  $R_L$  used at the output of the receiver coil, there is a voltage drop across the resistance and is given by  $V_2$  in equation (35). The

output voltage across the load  $V_2$  is less than the open circuit receiver coil voltage  $V_{th}$  and accounts for positive voltage regulation. The percentage voltage regulation is given by equation(37). The change in output voltage across the receiver coil from no load to full load, represented on a phasor diagram and is shown in Fig.9.

$$\frac{V_{th} - V_2}{V_2} \times 100\% = \frac{I_2 \operatorname{Re}(Z_{ou}) + I_2 \operatorname{Im}(Z_{ou})}{V_2} \times 100\% \tag{37}$$

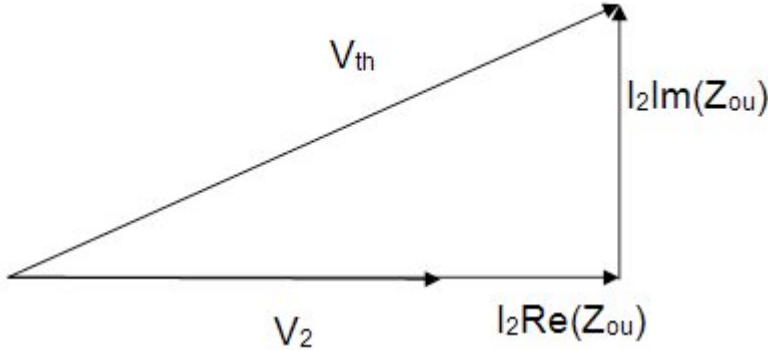
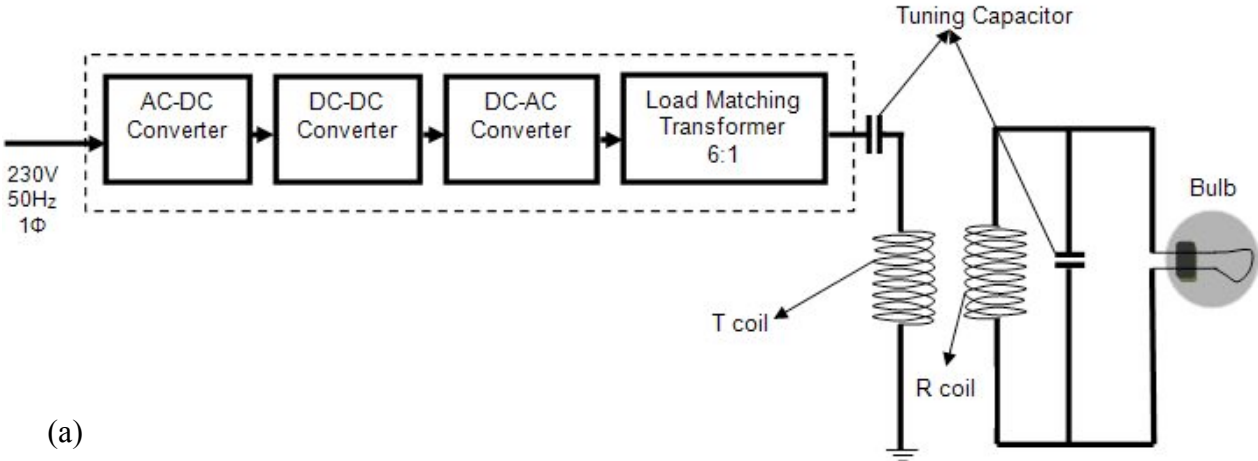


Fig. 9.Phasor diagram for voltage regulation.

**5. Experimental System**



(a)

(b)

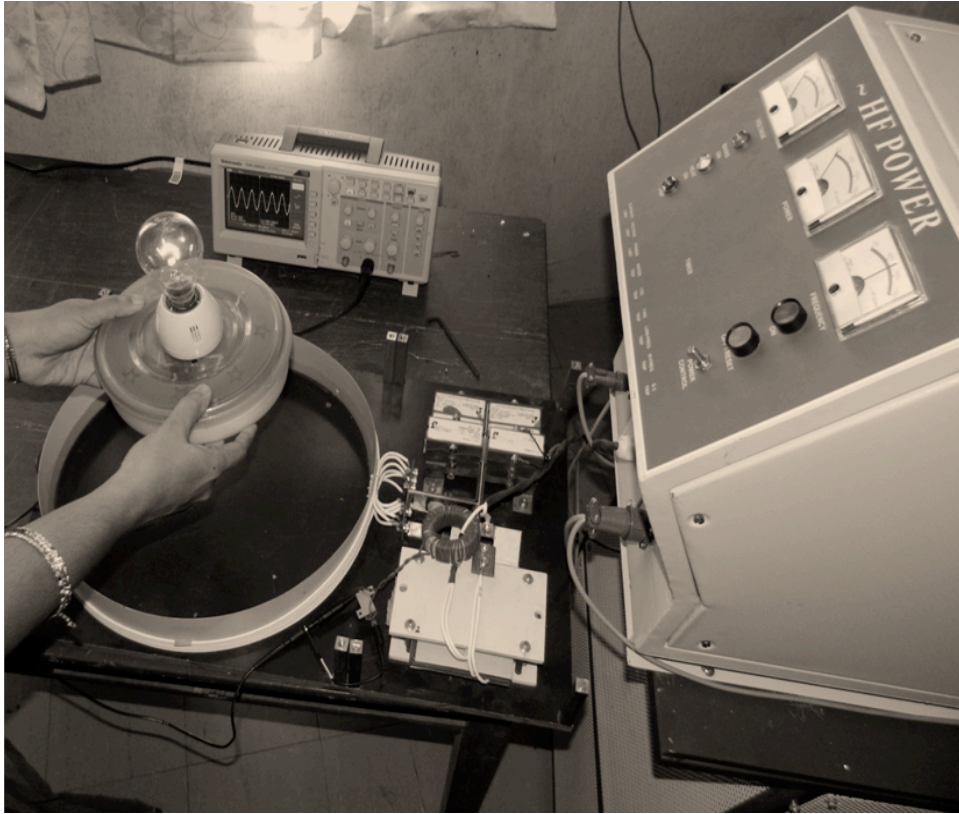


Fig.10.(a) The schematic of experimental setup with RF power supply of a resonant inductive wireless power transfer system.

(b). Resonant inductive wireless power transfer system powering a light load of 100W.

The analytical model of the wireless power transfer system described in Section 4 was tested with the experimental setup shown in Fig.10 (a) and (b) (Hema Ramachandran *et al* 2013) . The system consists of an RF power supply unit, transmitter coil, capacitors for tuning the transmitter coil, receiver coil with tuning capacitors and a light load of 230V,100W.The RF power supply system used an AC-DC converter, DC-DC converter for switching at 1.2MHz , DC-AC converter for inversion( Sahu, S *et al*, 2006) and a 6:1 load matching transformer( Jha M *et al*, 2013). The output of the load matching transformer is fed through series capacitors to the transmitter coil. The transmitter coil employed a helical solenoid geometric construction used 8 parallel Litz conductors forming a single turn each of cross sectional area 2.5 sq.mm and was wound on a wooden bobbin of diameter 35cm and length 0.8cm. The transmitter coil was forcefully resonated at 1.2 MHz by connecting it to 0.016 $\mu$ F capacitors in series. The receiver coil also employed Litz conductors of diameter 18cm and length 0.3cm was wound with 5 turns of wire in series having the same cross sectional area as that of the transmitter coil. The receiver coil was force resonated at 1.2MHz by connecting across it 1.4nF capacitance formed using four numbers of 0.01  $\mu$ F capacitors in series. The maximum current flow in the receiver coil was

limited to about 0.8A. The receiver coil was attached to a 100W, 230V bulb as the resistive load with a resistance of 530Ω. The receiver coil was set to varying coil positions in coaxial orientation from the transmitter coil at distances 0, 10, 20 and 30cm thereby varying the power transferred to the load and efficiency of power transfer.

### 5.1. Results and discussion

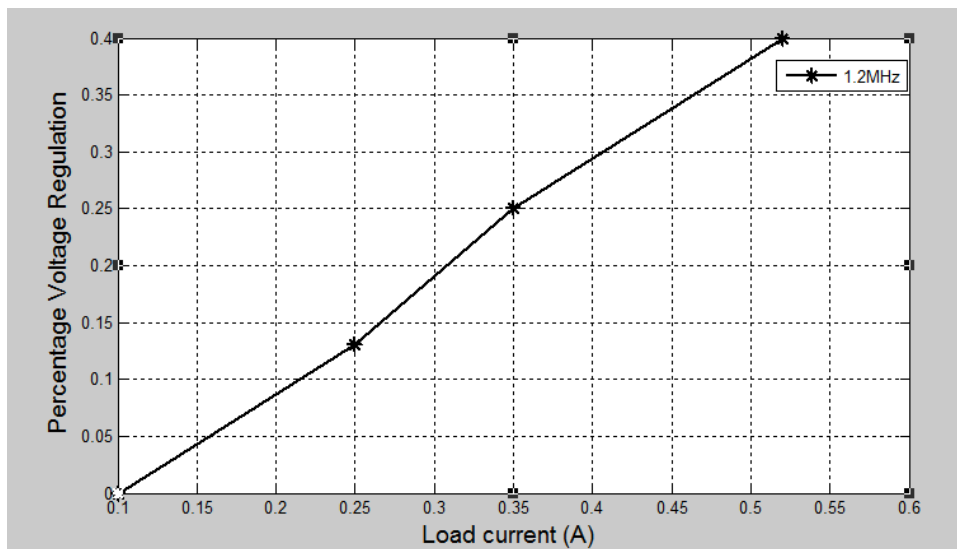
The extracted coil parameters of the transmitter and receiver coil at 1.2MHz are presented in Table II.

Table II. Extracted Coil Parameters

Parameters		Transmitter coil	Receiver coil
Self- Inductance	$L_T, L_R$	1.01 $\mu\text{H}$	12.05 $\mu\text{H}$
Self-Capacitances	$C_T, C_R$	0.017434 $\mu\text{F}$	1.4613 nF
Resistance	$R_T, R_R$	0.2 $\Omega$	0.3 $\Omega$
Unloaded Quality factors	$Q_T, Q_R$	76.11	452.53

The power input from the RF power supply was adjusted to develop a voltage input of 546V across the transmitter coil. The open circuit voltage across the receiver coil was measured with a potential transformer having a turn ratio of 20 before and after loading. The current flowing through the load was measured using a current transformer with a turn ratio of 5. The experimental plots are presented in Fig.11(a), (b) and (c).

(a)



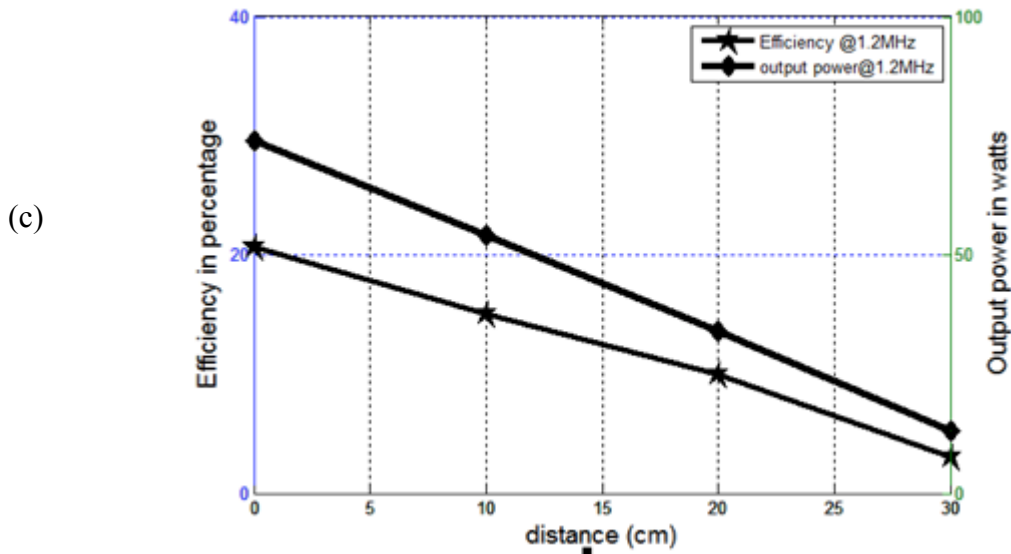
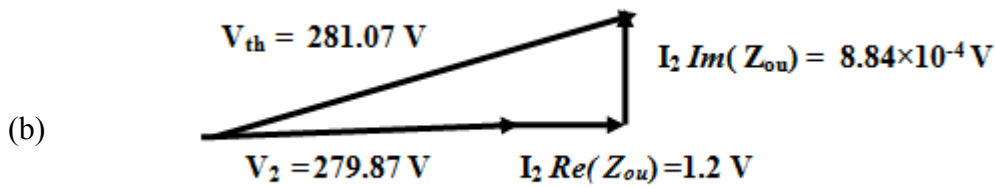


Fig. 11 (a).Variation of percentage regulation with load current.  
 (b) Phasor diagram of voltage regulation with maximum load current of 0.528A.  
 (c) Plot of efficiency and output power with distance of the receiver coil.

The Thevenin open circuit voltage across the receiver coil at no load with coaxial distance is 281.15V , while with load it drops to 279.87V corresponding to a positive maximum percentage regulation of 0.4 %. The maximum efficiency as obtained from the experiment also coincided with coaxial distance and was 20.62% when power transferred to the load is 73.89W, The resistive light load glows bright. As distance increased, the current through the load drops to about 0.18A at 30cm distance as the evanescent near field dies down drastically. At a distance of 20 cm, the open circuit voltage drops to 74.95V while the voltage across the load becomes 74.92V. The efficiency at 20cm distance was 9.92%. The percentage voltage regulation was also very negligible (Hema Ramachandran *et al* 2012) corresponding to a load current of 0.18A. The efficiency dropped to 3% at a distance of 30 cm at which the power transferred to the load was only 9.13W, where the lamp showed a minimal flicker. The voltage regulation in resonant wireless power transfer was similar to a conventional terminal transformer with resistive loading.

The drop across the load and the resistive part of the output impedance was predominant over the reactive drop across the output impedance. The pre-determined theoretical values were within 1% of the experimental results.

## 6. Conclusion

Voltage regulation study has been conducted on the experimental forced resonant inductive wireless power transfer system using a high frequency reflected impedance terminal analytical model. A resistive load attached to the system model shows a voltage regulation which increased with load current. The model can be experimented on capacitive and inductive loads as well. With inductive and capacitive loads the real part of the output impedance may lead or lag the output voltage which can lead to a drift in resonant frequency and lowering of power transfer efficiency. Hence it might be necessary to retune the external capacitances that terminate the receiver coil for realizing resonant power transfer. This requires advanced control circuitry and is a scope for further work in this area.

## Acknowledgement

The first author acknowledges the Speed-IT fellowship of the Government of Kerala, India. The authors also thank the funding grant from the Kerala State Council for Science, Technology and Environment.

## References

1. Alanson P. Sample, David A. Meyer and Joshua R. Smith (2010) "Analysis, experimental results and range adaptation of magnetically coupled resonators for wireless power transmission," *IEEE Trans. Ind. Electron.*, pp.1-11.
2. Mizuno T, Yachi S, Kamiya A, Yamamoto D (2011) "Improvement in Efficiency of wireless power transmission of Magnetic Resonant Coupling using Magneto plated wire", *IEEE Trans. Magnetics*; vol.47, issue 10, pp. 4445-4448.
3. J.G.Zhu *et al* (1996) "A generalized dynamic circuit model of magnetic cores for low and high frequency applications, *IEEE Trans. Power Electronics*, vol.11, no.2 , pp-251-259.
4. C.S. Wang *et al* (2004) "Power transfer capability and bifurcation phenomena of loosely coupled inductive power transfer systems", *IEEE Trans. Ind. Electron.* vol. 51, no.1, pp.148-157.
5. O.H. Stielau *et al* (2000) "Design of loosely coupled inductive power transfer systems", in Proc. Int. Conf. Power Syst. 4-7 December, Perth, pp.85-90.

6. J. E. Clem(1927) “Mechanical forces in Transformers.” *Trans. IEE*, 1927.
7. Marian K. Kazimierczuk, “High frequency magnetic components,” John Wiley & Sons, New York, 2009.
8. Kang Lin, Keith E. Holbert (2009) “ Applying the equivalent pi circuit to the modeling of hydraulic pressurized lines", *Trans. IMACS, Elsevier*; vol.79, issue 7, pp.2064-2075.
9. Hema Ramachandran, Bindu G.R (2013) " Wireless powering of Utility Equipments in a Smart Home Using Magnetic Resonance”, Proceedings of the IEEE International Conference on Recent Advances in Intelligent Computational Systems (RAICS), December, Trivandrum, 19-21, Kerala, India
10. Jha. M, Qureshi, M.F, Srivastav. P (2013) " Design of adaptive grey fuzzy PID controller with variable prediction step-size for power system dynamic stability control and its on-line rule training", *A.M.S.E Journals, Advances C*, vol.68, issue 1, pp. 1-21.
11. Sahu, S, Chandra S, Chkrabarthi B, Pal R.R (2006) " A high frequency low voltage current voltage controlled oscillator using modified emitter coupled logic (ECL) inverters", *A.M.S.E journals, Advances C*, vol.61, issue 3, pp. 1-20.
- 12.Hema Ramachandran, Bindu G.R (2012) “Wireless Charging of Lighting Gadgets using Low Q Resonant Coupling”, Proceedings of the International Conference on Advances in Computing, Communications and Informatics , pp.275-278, 3- 5, August, Chennai, India.